Measuring thermal conductivity in freezing and thawing soil using the soil temperature response to heating

P. P. Overduin*, D. L. Kane, W. K. P. van Loon

*Corresponding author: phone : +49-331-951-3720, fax: +49-331-288-2173, email: fsppo@uaf.edu

Abstract

The thermal conductivity of the thin seasonally freezing and thawing soil layer in permafrost landscapes exerts considerable control over the sensitivity of the permafrost to energy and mass exchanges at the surface. At the same time, the thermal conductivity is sensitive to the state of the soil, varying, for example, by up to two orders of magnitude with varying water contents. *In situ* measurement techniques perturb the soil thermally and are affected by changes in soil composition, for example through variations in thermal contact resistance between sensor and soil. The design of a sensor for measuring the temperature of the soil rather than the axial heating wire temperature has consequences for the modeling of heat flow. We introduce an approximation of heat flow from a heated cylinder with thermal contact resistance between the cylinder and the surrounding medium. This approximation is compared to the standard line source approximation, and both are applied to data measured over a one-year period in northern Alaska. Comparisons of thermal conductivity values determined numerically using the line source solution, line source approximation and the analytical form of the heated cylinder model fall within 10% of accepted values, except for measurements made in pure ice, for which all methods of calculation under-predicted the thermal conductivity. Field data collected from a complete freeze-thaw cycle in silty clay show a seasonally bimodal apparent thermal conductivity, with a sharp transition between frozen and thawed values during thaw, but a three-month transition period during freezing. The use of soil composition data to account for changes in heat flow due to the effect of latent

heat during phase change results in a relationship between soil thermal conductivity and temperature.

Keywords: thermal properties, instrumentation, transient heat pulse, frozen soil, permafrost

1 Introduction

The seasonal depth and duration of the active layer in permafrost regions is critical for biological, hydrological and mineralogical processes, as are the intensity and frequency of freezing and thawing events. The thermal conductivity of the shallow surface layer, which thaws and freezes seasonally, is used in the determination of surface heat balance. Various models of the surface energy balance use the thermal property of conductivity to predict the depth of thaw or freezing of the active layer by assuming a bimodal winter and summer thermal conductivity values. Such models (e.g. Anisimov et al., 1997; Hinzman et al., 1998) predict heat transfer, freeze/thaw depth and permafrost stability using these thermal conductivities. Treatment of geothermal data to recover heat flux histories also benefits from observed thermal conductivity data (Beltrami, 2001). Since spatial and temporal variations in soil thermal properties are dramatic (Hinzman et al., 1991; Putkonen 1998), they must be understood to adequately model physical processes.

Estimates of soil thermal conductivity are based either on models, summarized by Farouki (1981) or on experimental data. Goodrich (1986) measured the thermal conductivity of active layer soils at four Canadian locations using a transient heat pulse probe. His data indicated that this bimodal model is too simple and that the thermal conductivity values in such diverse soil materials as peat and gravel do not show the expected seasonal variation in thermal response. He concluded that, at depths shallower than about 1.0 m, estimates of thermal conductivity based on a simple bimodal, frozen-thawed model could be grossly in error, while interannual seasonal variations in thermal conductivity are probably acceptable below a depth of about 0.5 to 1.0 m. Smith and Riseborough (1985) investigated the effect of assuming a single frozen thermal conductivity value on the predicted temperature of the subsurface and found that it led to an over-prediction of the phase change boundary depth. The thermal conductivities of the shallow surface layers are highly dependent on the composition and state of the soil and vegetation. Changes in water and ice content produce the greatest changes (by a factor of ten or more) in thermal conductivity temporally (Yoshikawa et al., 2003) and generally correspond to drying/wetting or freezing/thawing events. Soil composition in the periglacial landscape is highly variable spatially due to the agency of cryoturbation. There remains a need for *in situ* measurements of thermal conductivity in these soils to determine the influence of water and ice dynamics on the thermal conductivity. Our objective is to present an improved model for heat flow around a linear heat source in which the radial temperature difference between two points in the soil is measured. We demonstrate the use of this model in the laboratory and for field measurements at temperatures close to phase change in freezing and thawing soils.

2 Models of transient methods for measuring thermal conductivity

2.1 Heat transfer model

Transient methods for the measurement of thermal conductivity have a long history (e.g. van der Held, 1949). Most field measurements of thermal conductivity are made using heated wire or needle probes modeled as perfect line conductors. The heat flux can be represented as a solution to the conduction equation in radial coordinates:

$$\frac{\partial^2 T}{\partial r^2} + \frac{1}{r}\frac{\partial T}{\partial r} = \frac{1}{\kappa}\frac{\partial T}{\partial t}, \qquad b < r < \infty \qquad (1)$$

where r is the radial dimension, b is the radius of the linear heat source, t is time, T is the temperatures of the medium, κ is the thermal diffusivity. Solutions are subject to the conditions:

$$T(r,0) = T_s(r,0) = 0, \qquad t = 0 \qquad (2)$$

For a cylindrical region within in a medium, the heat flux across the cylinder surface is equal to the heat flux leaving the cylinder surface:

$$-k\frac{\partial T}{\partial r}=H(T_s-T)\,, \qquad r=b,\ t>0 \qquad (3)$$

where we have introduced the thermal conductivity, k, of the region $r > b$, H, the thermal surface conductance at $r = b$ and the temperature of the sensor, T_s. The heat flux into the medium must be given by:

$$-k\frac{\partial T_s}{\partial r}(2\pi b)=q-C_s\frac{\partial T}{\partial t}\,, \qquad r=b,\ t>0 \qquad (4)$$

where the heat produced within the cylinder per unit length and time is given by q and the heat capacity of the cylinder per unit length is given by C_s.

2.2 Line source solution

Data from heated wire or needle probes are usually modeled on a solution for an infinite line heat source (Lachenbruch, 1957) in a homogeneous, isotropic medium. For a continuous line source, the measured temperature difference between two radial points r_1 and r_2 is given by:

$$\Delta T(t)=\frac{q}{4\pi k\Delta r}\int_{r_1^2/4\kappa t}^{r_2^2/4\kappa t}\frac{e^{-u}}{u}du \qquad (5)$$

where q is the heat production of the central heating wire [W m^{-1}], k is the thermal conductivity of the medium [W m^{-1} K^{-1}], Δr is the radial distance over which the temperature difference is measured [m], κ is the thermal diffusivity of the medium [m^2 s^{-1}] and u is an integration variable. In most field measurements in soil, a needle probe with a thermistor or thermocouple embedded in the probe is heated with some known power, and the temperature response of the probe is measured as a function of time. An approximation of the solution is usually used to treat data for the heating curve of the needle:

$$T(r,t)=\frac{q}{4\pi\lambda}\left\{\ln\left(\frac{4\kappa}{\gamma b^2}\right)+\ln t+\frac{1}{1\cdot 1!}\frac{b^2}{4\kappa t}-\frac{1}{2\cdot 2!}\left(\frac{b^2}{4\kappa t}\right)^2+O\left(t^{-3}\right)\right\} \qquad (6)$$

where γ is Euler's constant (0.5772156649), λ is the bulk thermal conductivity of the medium [W m^{-1} K^{-1}], and the Landau symbol, $O(t^{-3})$, indicates that the absolute value of the error in the approximation is less than some constant times t^{-3} at large enough t. At large times, it is assumed that $b^2/4\kappa t$ is sufficiently small to lead to a linear dependence on ln t:

$$T(r,t) = \frac{q}{4\pi k}\ln t + \mathrm{c(r)}$$

Since the measurement takes place at a fixed position the second-term function of r can be treated as a constant. Applied to the radial temperature difference this assumption results in an expression independent of time for the heating curve:

$$\Delta T = \frac{q}{2\pi k}\ln\left(r_2/r_1\right), \qquad r_{1,2}^2/4\kappa t << 1 \tag{7}$$

the expression for the cooling curve becomes:

$$\Delta T\left(t > t_s\right) = \frac{q}{16\pi k\kappa}\left(r_1^2 - r_2^2\right)\frac{t_s}{t\left(t_s - t\right)}, \qquad r_{1,2}^2/4\kappa\left(t - t_s\right) << 1 \tag{8}$$

where $t = t_s$ is the time at which power to the heating wire is switched off. For both approximations, the terms in $r^2/4\kappa t$ must be small.

2.3 Medium bounded internally by cylindrical region

Relevant analytic solutions are also available for a region bounded internally by a cylinder (Carslaw and Jaeger, 1990), and for a region bounded internally by a cylinder with contact resistance (Kristiansen, 1982). Generally only the temperature of the cylinder is considered, reflecting the usual sensor design. The heated cylinder is assumed to be of infinite length (heat flow is restricted to the radial direction) and to act as a perfect conductor (no axial effects of heating). Jaeger (1956) provides solutions for a number of scenarios and investigates the effect of thermal contact resistance on the temperature of the cylinder. Blackwell (1954) examined the effect of contact resistance between the sensor and the medium, but also restricted his analysis to the temperature of the heat source. Van Loon et al. (1989) present a second order time correction to the needle probe model that better describes its behavior at short times. For any system measuring the temperature of the medium, expressions for T rather than T_s are required. The temperature of the medium is determined under the conditions $T(r, 0) = T_0$ and a constant heat supply to the region $r < b$ for times $t > 0$. Based on Blackwell's work, Kristiansen (1982) provided a solution for the temperature field in the medium:

$$T(r,t) = \frac{\alpha q b^2}{k}\int_0^\infty \left(1 - e^{\tau u^2}\right)\frac{\left(RJ_0(u\eta) - PY_0(u\eta)\right)}{u^2(P^2 + R^2)}du \qquad (9)$$

where u is the integration variable, exp is the exponential function and

$$P = uJ_0(u) + k\left(hu^2 - \alpha\right)J_1(u) \qquad (10a)$$

$$R = uY_0(u) + k\left(hu^2 - \alpha\right)Y_1(u) \qquad (10b)$$

where J_z and Y_z are the zth order Bessel functions of the first and second kinds, respectively. We have introduced the dimensionless parameters:

$$h = k/bH \qquad (11a)$$

$$\eta = r/b \qquad (11b)$$

$$\tau = 4\kappa t/b^2 \qquad (11c)$$

$$\alpha = 2\pi b^2 \rho C/S \qquad (11d)$$

where h is a contact resistance term, η is the dimensionless radius, τ is the dimensionless time and α is twice the ratio of the volumetric heat capacity of the medium, ρC, to that of the sensor, $S/\pi b^2$, where ρ and S are the density of the medium and the heat capacity of the sensor per length. As H takes on large values, the solution reduces to that of the heated cylinder without thermal contact resistance. The temperature distribution in the medium depends in a non-linear fashion on the physical parameters. Its integral form requires numerical solution, although DeVries and Peck (1958a) provided a large time approximation, which is considered below.

2.4 Large time approximation of the medium temperature

DeVries and Peck (1958b) applied Blackwell's (1954) approach to generate a large-time approximation for the temperature of the medium:

$$T(\tau,\eta) - T_0 = \left(\frac{q}{4\pi k}\right)\left[\ln\tau - 2\ln\eta - \gamma + \frac{2}{\tau}(\ln\tau - \gamma) + \frac{1}{\tau}\left(1 - 2\ln\eta + \eta^2\right) + O\left(\tau^{-2}\right)\right] \quad (12)$$

where γ is Euler's constant. The assumptions that no phase change occurs and that no thermally induced migration of water or vapor occurs are implicit. These assumption are addressed in the discussions of results. For application to the sensor that we use, expressions for the temperature difference between $\eta_1 = r_1/b$ and $\eta_2 = r_2/b$ are obtained for the heating curve:

$$\Delta T(t) = \left(\frac{q}{4\pi k}\right)\left(2\ln\frac{\eta_1}{\eta_2} + \frac{1}{\tau}\left(2\ln\frac{\eta_2}{\eta_1} + \eta_1^2 - \eta_2^2\right)\right) \quad (13)$$

After τ_s heating is switched off. The corresponding cooling curve reads as:

$$\Delta T(t) = \left(\frac{q}{4\pi k}\right)\left(\frac{\tau_s}{\tau(\tau_s - \tau)}\left(2\ln\frac{\eta_2}{\eta_1} + \eta_1^2 - \eta_2^2\right)\right) \quad (14)$$

For this approximation to order τ^{-2}, dependence of the temperature response on the thermal contact resistance disappears (DeVries and Peck, 1958a). As the thermal heat capacity of the medium or the effective sensor radius approach zero, these solutions reduce to the solutions given by the line source approximation. For the heating curve, we can reformulate the temperature difference as:

$$\Delta T(t) = A\frac{1}{t} + B \quad (15)$$

where:

$$A = \frac{qb^2}{16\pi k\kappa}\left(2\ln\frac{\eta_2}{\eta_1} + \eta_1^2 - \eta_2^2\right) \text{ and } B = \frac{q}{2\pi k}\ln\left(\frac{\eta_2}{\eta_1}\right) \tag{16}$$

so that a means of calibrating for the effective sensor properties using measurements in materials of known thermal properties is provided. For the cooling curve, the same *A* appears in the temperature drop:

$$\Delta T(t) = A\frac{t_s}{t(t-t_s)} \tag{17}$$

As for the line source approximation, the use of the medium temperature results in the cancellation of terms in the ratio of radial distances for the cooling curve.

2.5 Sensitivity

To evaluate the sensitivity of sensor output to changes in parameter values, we express the temperature of the medium (equation 9) in a form corresponding to the sensor output as a function of time only:

$$\Delta T(t) = \frac{\alpha q}{\pi b^2 k}\int_0^\infty \left(1 - e^{\tau u^2}\right)\left(R\Delta_J - P\Delta_Y\right)\left(u^2(P^2 + R^2)\right)^{-1} du \tag{18}$$

where:

$$\begin{aligned} \Delta_J &= J_0(u\eta_1) - J_0(u\eta_2) \\ \Delta_Y &= Y_0(u\eta_1) - Y_0(u\eta_2) \end{aligned} \tag{19}$$

The sensitivity of the temperature to parameter β_i is given as:

$$\chi_i = \beta_i \frac{\partial T(t, \beta_1, \beta_2 ... \beta_n)}{\partial \beta_i} \tag{20}$$

for surface conductance, the sensitivity is expressed as:

$$\begin{aligned} \chi_H &= H\frac{\partial T}{\partial H} \\ &= \frac{-2q\alpha}{\pi b H^2}\int_0^\infty \left(1 - e^{\frac{\kappa t u^2}{b^2}}\right)\left(\frac{\Delta_J Y_1(u) - \Delta_Y J_1(u)}{(P^2 + R^2)} - \frac{2R\Delta_J - 2P\Delta_Y}{(P^2 + R^2)^2}\right) du \end{aligned} \tag{21}$$

and η_1 and η_2 are the dimensionless radii at which temperature difference is measured. The condition for the simultaneous identification of parameter values from a time series of temperature data is the linear independence of the sensitivities over the time period (Beck and Arnold, 1977). The analytical solution is non-linearly dependent on the parameters, β_i, and a condition for identifiability is not evident. We calculated the sensitivity of the temperature gradient numerically for the five parameters, *b*, *S*, *H*, *k*, and κ, as a function of time since the start of heating using the adaptive Lobatto quadrature technique and integration limits of 1 x 10^{-3} and 10. The oscillatory nature of the integrands required a maximum function count limit of at least 1 x 10^{6} to prevent early termination of the integration (Gander and Gautschi, 1998). For the probe radius, heat capacity and heat production used here (b = 8 x 10^{-5} m, S = 131 J m^{-1} K^{-1}, q = 1.5 W m^{-1}), with the parameter values of k = 0.3 W m^{-1} K^{-1}, and κ = 2.5 x 10^{-7} m^2 s^{-1}, the temperature gradient is less sensitive to contact resistance or probe radius and thermal mass than to medium thermal conductivity or diffusivity by a factor of over 100 as time approaches 180 s (Figure 1). H^{-1} was set to zero for the other five sensitivities, and to 3000 W K^{-1} for χ_H. Parameter values were chosen to match sensor characteristics. The magnitude and the general shape of the sensitivities do not change over a range of k, κ and *H* values extending beyond that encountered in the soil. Increases in thermal diffusivity and thermal surface conductance both increase the temperature gradient at short times (< 10 s). Thus, large changes in *H* and small changes in κ will affect the shape of the temperature gradient response to heating in a similar fashion. The thermal conductivity influences the temperature gradient more with increasing time, in a near linear fashion after 20 s. The large time approximation can be expected to deliver thermal conductivity, but does not contain recoverable information on the probe characteristics or thermal surface conductance. Repeated numerical solution of the integral solution is computationally costly. In the following, we compare use of the large time approximations for the line source and heated cylinder solutions.

3 Methods

3.1 Radial and axial temperature measurements

Transient heat pulse sensors of any design share some basic characteristics. Simultaneous measurements of the heating power and either the axial temperature, the medium temperature at some radial distance or the temperature drop between radial positions over time are compared to some model for heat flow, making it possible to calculate the effective thermal properties of the medium. For all designs, power requirements are theoretically adjustable, and modest enough to permit battery operation over long periods, an advantage for remote sites. The radial sensor also differs from axial probes in that the temperature around the heat source is monitored rather than the temperature of the heat source. This design confers the advantage that less power is required since thermopile sensitivity to small variations in thermal gradient is greater than most thermistor or thermocouple resolutions. By measuring the temperature difference between two points, higher accuracy and lower susceptibility to drift can be achieved than for absolute temperature measurements. The thermopile also averages the radial temperature gradient over some axial length (and for the sensor we use, over two angular directions), minimizing the influence of localized heterogeneities on heat flow. For axial sensors, a thermal contact resistance is created when the temperature sensor is embedded within the heat source (Cull, 1978). Measuring the temperature of the medium at some distance from the heat source partially avoids this problem, and provides a wider range of scales over which the thermal conductivity may be measured. Disadvantages include the enhanced potential for contact resistance between the sensor and the medium, since the sensor’s area is quite large compared to the more common needle probe, and a reduced ruggedness, since the film containing the thermopile must necessarily have low thermal conductivity and heat capacity.

3.2 The transient sensor

We use the TP01 sensor manufactured by Hukseflux Thermal Sensors, which consists of a doubled heating element (diameter: 2 x 10^{-5} m; length: 0.06 m) embedded in a thin film, in which a radially-oriented thermopile has also been integrated (Figure 2). The heating wire extends 20 mm beyond the thermopile in both axial directions to ensure radial heat flow across the thermopile. The thermopile measures the difference in temperature between two points 1 and 5 mm from the line source, averaged over 20 mm. Averaging also occurs over thermopiles on either side of the heating wire.

The difference in temperatures is related to the thermopile output by a calibration factor determined via a one-point calibration in an agar-water solution, in which the agar gel prevents convective heat transfer. The modeled temperature holds under the assumptions that the medium is well characterized by a thermal conductivity at the measurement scale, isotropic and homogeneous; that heat flow is steady, conductive and radial, and is not subject to any contact resistance at the sensor-medium interface. A typical calibration factor is 6.3 x 10^{-5} V K^{-1} (Hukseflux, 2000). The CR10X datalogger has a 1 μV resolution, which corresponds to a temperature gradient resolution of about 4 K m^{-1}. This corresponds to a mean uncertainty in k of 0.01 W m^{-1} K^{-1} over the k range of 0.3 to 4.0 W m^{-1} K^{-1}, assuming that uncertainties in heat production, thermopile position and measurement times are negligible. The thin film encasing the sensor’s heating wire and thermopile introduces a minimum thermal surface conductance. It has a thermal conductivity of 0.2 W m^{-1} K^{-1} and is about 1.5 x 10^{-4} m thick, leading to an conductance of at most H = 3000 W m^{-2}. The temperature dependencies of both the heating wire resistance and thermopile output are possible sources of systematic error. The heating wire resistance varies less than 0.04 % K^{-1} over the temperature range -20 to 20 °C and is neglected. We assume that the opposition of the warm and cold junctions compensates for the first order temperature dependency of the thermopile.

To estimate the thermal conductivity of a sample, the sensor is installed in the sample and a current of measured voltage flows through the heating wire for a period sufficient to establish a “steady” reading. Thermopile output is measured before, during and after heating. In soils, heating typically lasts for 180 s and the temperature gradient is monitored for an additional 180 s after heating ceases. This produces a time series of data during heating and cooling, both of which can be used to estimate soil thermal properties.

3.3 Field methods

We have collected data from a site in the northern foothills of the Brooks Range in Alaska (68° 29´ N, 149° 29´ W). The site lies in the Galbraith Lake valley, and is located in lacustrine deposits partially reworked by streams draining into Galbraith Lake as the shoreline receded. The site is thus poorly drained and the water table is within 20 cm of the ground surface during the growing season. The soil is assumed to remain saturated during freezing and thawing. Landcover type is classified as moist non-acidic tundra, the soil pedon is classified as a cryaquept and the soil horizons are contorted by cryoturbation (Ping, 1998). Permafrost temperatures at 20 m are about –5 °C (Osterkamp 2003).

Installation of sensors followed careful excavation of a soilpit. Soil was removed by horizon, and replaced and compacted to close to the original density. Sensors were installed in undisturbed soil in the pit wall. The thin film of the thermal conductivity sensors here requires careful insertion; we used a thin knife blade to insert the sensor in to the soil, a method which has the potential to create gaps around the sensor. The soil here is subject to frost heave, and since data here are collected after one complete freeze-thaw cycle, it is assumed that the soil has compacted. Measurements considered in this study were taken from sensors installed in a silty clay soil at 0.37 m below the ground surface. Soil at this location had an oven-dry (105 °C) bulk density of 0.5 g cm^{-3}, with less than 3% carbon content and particle size percentages by weight of 42% clay, 45% silt and 13% sand (Soil Survey Staff, 2005).

In field deployment north of the Artic Circle in Alaska, a datalogger (CR10X, Campbell Scientific Inc.) controlled relays connecting the heating wire to the power source. In remote field installations, a 12 V battery recharged continuously by a 50 W solar panel was the electrical source for the heating wires. The power requirements for frequent measurements were met by this system (including a meteorological station with TDR unit), with enough reserve power to continue measuring through the winter darkness. The datalogger also measures heating power and thermopile voltage. Data in the field were analyzed using the line source approximation, following the manufacturer's recommendations, and cooling curves were recorded for later reference, whereas in the laboratory, the heating and cooling curves were saved for post-processing.

3.4 Soil state

Two thermistors measured temperature proximal to the thermal sensors on an hourly basis. The thermistors were calibrated using a de-ionized water-ice mixture, from which a thermistor-specific offset, δ_o, for the Steinhardt-Hart equation was generated:

$$1/T = 1.28\times10^{-3} + 2.37\times10^{-4}\left(\ln\left(R_T - \delta_o\right)\right) + 9.06\times10^{-8}\left(\ln\left(R_T - \delta_o\right)\right)^3 \qquad (22)$$

where R_T is the measured resistance and δ_o is the resistance offset at 0 °C. A linear interpolation of the soil temperatures was performed to estimate the temperature at the sensor location. The thermistors were located 0.05 and 0.12 m from the thermal conductivity sensor. Liquid water content was also measured proximal to the thermal sensors on an hourly basis using time domain reflectometry to measure the bulk apparent dielectric constant of the soil. Topp et al.'s equation (1980) was used to calculate volumetric liquid water contents in thawed soil. Van Loon et al. (1991) showed that Smith and Tice’s (1988) empirical frozen soil calibration could be explained by assigning a lower relative dielectric permittivity to the unfrozen water remaining in the frozen soil. We use his relationship here to calculate the unfrozen water content of the frozen soil. TDR accuracy for volumetric water content is estimated to be better than 5% following Roth and Boike (2001).

3.5 Data analysis

In the following, sensor output is referred to as the temperature gradient. For both of the large time approximations, it is assumed that $t >> r^2/4\kappa$. Soil κ values are expected to vary between 1.2 x 10^{-7} and 1.4 x 10^{-6} m^2 s^{-1} (Yershov, 1990), so that t >> 2 to 0.2 s for r_1 = 0.001 m. We consider this condition to be satisfied at t > 100 s. Field data are analyzed using the line source approximation, and the heated cylinder approximation. For the latter, the slope of the temperature drop data against inverse time is found:

$$A = \frac{qb^2 C_{app}}{16\pi k_{app}^2}\left(2\ln\frac{\eta_2}{\eta_1} + \eta_1^2 - \eta_2^2\right)$$

The probe-dependent terms are collected to provide:

$$A = E_\circ \frac{qC_{app}}{k_{app}^2} \tag{23}$$

where

$$E_\circ = \frac{b^2}{16\pi}\left(2\ln\frac{\eta_2}{\eta_1} + \eta_1^2 - \eta_2^2\right) \tag{24}$$

is a probe constant. Estimates of the apparent heat capacity of the soil, C_{app}, at the time of measurement are generated from field soil composition data:

$$C_{app} = C + L_f \rho_w \frac{d\theta_w}{dT} \tag{25}$$

where C is the thermal heat capacity of the soil (Kay et al., 1981), and is calculated as the sum of the relative volumetric fraction-weighted heat capacity over the three phases ice, water and soil matrix (i, w, s):

$$C = \sum_{n=i,w,s} \rho_n C_n \theta_n \tag{26}$$

where ρ_n, C_n and θ_n are the density, specific heat capacity and volumetric fraction of the nth soil phase. θ_i was estimated based on porosity and changes in liquid water content during and after freezing. In doing so, we implicitly assume that ice segregation and moisture redistribution has a negligible effect on the composition of the measurement volume. Volumetric liquid water content was calculated as described in the methods section, and the soil matrix volume fraction was assumed to be equal to (1 - θ_{sat}), where the latter term is the volumetric liquid water content at saturation. The analytical solution to the heat flow equation (equation 9) cannot be used to measure the apparent thermal conductivity when the apparent thermal conductivity is strongly temperature dependent (Kay et al., 1981). This occurs when the liquid water content is strongly temperature dependent, generally at temperatures between -0.5 and 0 °C. The rate of change in liquid water content with temperature for both the freezing and thawing arms of the freezing characteristic curve can be given by an empirical relationship of the form:

$$\theta_w = F|T|^G + H \tag{27}$$

where θ_w is the volumetric liquid water content, F, G and H are constants (the offset, H, is introduced to better represent the freezing data), and $|T|$ is the absolute value of the temperature measured in °C. These values were used to calculate the release and consumption of latent heat as a function of soil temperature.

4 Results and Discussions

4.1 Sensor calibration

The radial temperature differences measured by the sensor while embedded in ice from degassed, distilled water, in agar gel, in moist clay and in dry sand are plotted as a function of time since the beginning of heating in Figure 3. For all four materials, the thermal gradient continues to increase with time throughout heating and its magnitude after 180 s is inversely proportional to the thermal conductivity of the medium. For high thermal conductivity materials, the thermal gradient approaches a linear rate of increase more rapidly during heating. The thermal gradient falls very rapidly for high k values and slower for low k values within three seconds of the cessation of heating and approaches zero as time increases. The manufacturer's suggestions recommend using the thermal gradient before and after 180 s of heating, $\Delta T(180) - \Delta T(0)$, for the determination of thermal conductivity. Use of the $\Delta T(0)$ term accounts for any thermal gradients at the onset of heating. This corresponds to the line source approximation, which represents the thermal gradient at large times, when the conditions in Equations 7 and 8 are satisfied, as a constant. Thermal conductivity values calculated for the sand, clay, ice and agar are shown in Table 1. The probe constant, E_o, for the heated cylinder is calculated using equation 24 and the accepted value for water and agar. This value is used to calculate the thermal conductivity for the other three materials. A manufacturer-supplied probe constant is applied for the line source approximation and line source fit. The heating curves of the same data are plotted in Figure 4 as a function of t^{-1}. Black symbols mark those values used to calculate the linear approximation, gray values are those neglected in the least squares fit. Earlier measured values were eliminated to maximize the coefficient of determination. More values are included for high thermal conductivity materials since the thermal gradient resolution decreases with increasing thermal conductivity and since materials higher in thermal diffusivity approach linearity as a function of the inverse time more rapidly. Thermal conductivity values using these methods, as well as the least squares fit to the line source model, and the large time approximation of the heated cylinder, are presented in Table 1. The line source solution values are found via least squares curve-fitting to numerical calculations of equation 5 with thermal conductivity as the fitting parameter. All methods of determination give values for the porous materials within the accepted range. Values for agar and for ice show greater deviation from the accepted values. The line source performs best for the agar, while the heated cylinder approximation comes closest to the ice value. The maximum deviation for the agar value is 7%, and 17% for the ice.

4.2 Field Data

Least squares fits of equation 27 to freezing and thawing data collected over three freezing and thawing cycles from late summer 2001 until summer 2004 are shown in Figure 5. Coefficient values are found using least-squares fitting (freezing: $\{F, G, H\}$ = {0.253, -0.572, 0.051}, $r^2 = 0.98$; thawing: $\{F, G, H\}$ = {0.169, -0.168, 0}, $r^2 = 0.93$). Hysteresis affects the water content at temperatures above -10 °C and may be result of at least three processes: solute exclusion from the forming ice increases the concentration of solutes in the remaining liquid water, depressing its freezing point; capillarity and the irregularity of the pore space cause hysteresis in a fashion analogous to that of wetting and drying curves and the soil solution may also super-cool before nucleation (Bittelli et al., 2003). The steeper slope of the thawing curve close to the freezing point results in higher apparent thermal conductivities for thawing soils than for freezing.

Figure 6 shows the soil temperature, volumetric liquid water content, apparent thermal heat capacity and apparent thermal conductivity as a function of time. The soil temperature at 0.32 m depth has begun to decrease by the beginning of September. The soil reaches a temperature close to 0 °C by September 12th and remains within 0.5

degrees of 0 °C for more than one month. During this period, warming of the air temperature between October 2nd and 10th lead to an increase of liquid water content relative to the pre-freezing saturation water content of 0.48 $m^3 m^{-3}$.

Bulk soil thermal heat capacity values between 2.2 and 3.0 MJ $m^{-3} K^{-1}$were calculated, which lie within the range for silt and sand soils given by Yershov (1990; 1.2 to 3 MJ $m^{-3} K^{-1}$). The apparent thermal heat capacity is shown in Figure 6, truncated to maximum values of 6 MJ $m^{-3} K^{-1}$. During fall freezing, C_{app} increases to over 800 MJ $m^{-3} K^{-1}$, probably due to the fact that measurement times were coincident with the soil having reached the melting point. Putkonen (2003) observed similar values in thermal heat capacity as a function of temperature, with values increasing rapidly as the temperature approached the melting point.

The apparent thermal conductivity of the soil shows a roughly bimodal seasonal variation, with lower values in thawed soil than in frozen. This is expected, as the thermal conductivity of ice is four times as high as that of water. Global climate models which incorporate permafrost usually estimate thaw depth based on bimodal seasonal variation in thermal conductivity between a thawed and frozen value. Laboratory measurements of thermal conductivity presented by Yershov (1990) and Hinzman (1998) show higher values (by factors of up to 2, depending on material and ice and water content) for frozen soils than thawed soils for a wide range of soil types, including silt, clays, sands and peats. Frozen and thawed soil thermal conductivity values are each very weakly dependent on temperature, primarily as a result of the temperature dependence of the thermal conductivity of water and ice. The transition from frozen to thawed value occurs at sub-zero temperatures. The apparent thermal conductivity data observed here show two departures from this model.

Apparent thermal conductivity spikes occur during spring thaw and during fall freezing, during which values increase from 1.0 and 1.4 W $m^{-1} K^{-1}$ to 1.3 and 2.8 W $m^{-1} K^{-1}$, respectively. There is a sharp discontinuity in the time series of apparent thermal conductivity, so that the duration of this spike can be estimated. It lasts 6 and 11 days in the spring and fall, respectively. In the fall, the spike occurs between temperatures of -0.5 and -1.1 °C, with liquid water contents between 0.4 and 0.35. During thawing, the spike begins at -1.9 °C and returns to a stable thawed value after soil temperatures reach 1.1 °C. The thermal conductivity of the soil close to the freezing point is usually assumed to take values close to those that may be interpolated from the frozen and thawed values at the same total water content (Hinzman et al., 1991).

Thawing occurs over a shorter time span than freezing. The soil temperature increases from -0.5 to +0.5 °C in less than one week, while the decrease from +0.5 to -0.5 °C occurs over more than one month. At this soil depth, the mean volume-normalized rate of freezing is -1.3 MJ d^{-1} over an 80-day period while the mean rate of thawing is 5.0 MJ d^{-1} over a 22-day period. Apart from the influence of different energy balances at the surface, thawing is speeded relative to freezing by the infiltration and refreezing of melt water from shallower horizons, and by the absence of an insulating snow layer. The line source approximation shows increased values of apparent thermal conductivity during phase change (Figure 6). The magnitude of the increase is greater during thawing than during freezing, probably owing to differences in the way phase change occurs.

The assumption that moisture redistribution does not occur in the soil after phase change begins is invalid in almost any freezing or thawing soil. Moisture is redistributed at a spatial scale larger than that of the sensor used here. For example, the downward percolation of meltwater in the upper soil profile to lower horizons with refreezing in spring (Ippisch, 2003) is a large scale process. However, at the sensor scale, this would be reflected in the measured thermal conductivity values. It is also possible that the heating required to measure thermal conductivity results in moisture redistribution at the scale of the sensor. Moisture is redistributed away from the heating wire radially by the temperature gradient created during heating (DeVries and Peck, 1958b). DeVries and Peck (1958b) examined moisture redistribution in response to heating using a needle probe by theoretical, numerical and experimental methods, and found that the absolute change in moisture content and the influence on measured thermal conductivity are small at temperatures below about 40 °C, and that the former approaches zero close to saturation. The magnitude of the redistribution depends on the temperature gradient produced, the duration of heating and on the hydraulic diffusivity of the soil. Since the heating period here is 180 s, heating power is less than 1 W and the hydraulic conductivity of the silty clay is low, this effect is ignored in the unfrozen soil. The hydraulic conductivity of frozen soil is orders of magnitude lower than that of the unfrozen soil (Burt and Williams, 1976; Kane and Stein, 1983). For the frozen soil, latent heat effects are likely to have a much greater influence than redistribution. Fuchs et al. (1978) showed theoretically that the effects of phase change on the apparent thermal conductivity are limited to a well-defined temperature range, between 0 and -0.5 °C for a Palouse loam. The lower limit of this temperature dependency is a function primarily of total soil water content (Fuchs et al. 1976; Kay et al., 1981). Thermal conductivity measurements in the frozen soil may also be affected by cumulative migration and freezing of water over multiple measurement cycles at the same position. Depending on where the induced temperature gradient and the amount of ice accumulated, the thermal conductivity would be increased over the course of multiple measurements. We cannot exclude this possibility, but the near one-to-one relationship between thermal conductivity and temperature below -10 °C suggests that it depends on liquid water content only, and not on measurement history.

Figure 7 shows the variation in apparent thermal conductivity calculated with the line source (a) and heated cylinder (b) models using the cooling curve data and the apparent heat capacity calculated via equation 25 as a function of soil temperature during two freezing and three thawing periods from May 18, 2002 until July 21, 2004. Cooling (grey circles) and warming periods (black crosses) are differentiated on the figure. The relatively stable apparent thermal conductivities calculated via the heated cylinder approximation when the soil was below -5 °C in the winters of 2002/2003 and 2003/2004 vary between 1.2 and 1.6 W m^{-1} K^{-1}. Both winters produce similar values as a function of temperature. The values calculated via the line source approximation vary as a result of varying temperature differences after 180 s of heating. Warming values above 0 °C in 2002 lie between 0.65 and 0.90 and increase to the range 0.90 to 1.05 W m^{-1} K^{-1} in the summer of 2004. The apparent thermal conductivity of the freezing and frozen soil changes slowly over time. The hysteresis-like difference between cooling and warming periods of the line source data is not directly related to the liquid water content of the soil, which is similar during the winters of 2002/2003 and 2003/2004. Both approximations result in slight increases in thermal conductivity with decreasing temperature below –10 °C, corresponding to increases in ice content. The rate of increase (0.009 W m^{-1} K^{-2}) in the heated cylinder thermal conductivity is somewhat lower than the rate of decrease in thermal conductivity of pure ice with temperature (0.011 W m^{-1} K^{-2}), probably as a result of the composite nature of the soil. Since ice segregation proximal to the sensor or an increase in contact resistance would lead to higher estimates of k at these temperatures, we suggest that this serves as indication that neither of these processes are operative. The freezing and thawing arms of the apparent thermal conductivity as calculated with the line source approximation (Figure 7a) converge to a narrower range of values as a function of temperature in the temperature range (-10, 0 °C) for the heated cylinder approximation (Figure 7b). This suggests that the influence of non-conductive processes on the heat flux within the measurement volume can be compensated for by accounting for the latent heat change associated with melting of soil pore ice alone. The thermal conductivity values calculated within this temperature range are therefore likely to be close to the true values.

5 Conclusions

We develop a large time approximation for the radial temperature gradient in a medium surrounding a cylinder with heat production. This approximation is used to model heat flow from a transient heat pulse thermal conductivity sensor while using a time series of heating data to calculate the apparent thermal conductivity of the soil. A commercially available sensor measuring the radial temperature gradient produced results comparable to the line source model. Based on the form of the heated cylinder model, thermal conductivity sensors that measure the radial temperature gradient, rather than the axial temperature, should be operated in a heating, rather than cooling mode. By including only first order term in time, terms with thermal surface conductance between the sensor and the soil cancel out for the radial temperature difference, suggesting an improvement over axial temperature measurements. Thermal conductivity calculated over a freeze-thaw cycle in the field showed roughly bimodal seasonal variation, with winter thermal conductivities 50 % higher than summer values. Using soil composition data to account for latent heat effects on thermal conductivity measurements leads to convergence of the freezing and thawing arms of the thermal conductivity data, suggesting that the values so obtained represent the actual bulk thermal conductivity of the soil.

This work underscores the importance of recording data on the composition of the soil in parallel with soil temperature, particularly at temperatures close to the freezing point. Soils in most permafrost landscapes typically spend well over a quarter of the year at temperatures between -5 and 0 °C, and this period is critical for many processes in the active layer (for carbon release, for example). The relationship between the bulk thermal properties of the soil and the temperature and moisture content of the soil will play a role in determining changes to the soil and permafrost as the climate changes. There remains a need for more thermal conductivity measurements under field conditions.

Acknowledgements

We thank Dr. K. Erbas and Dr. D. Stromeyer of the Geo-Research Center in Potsdam, Germany for fruitful discussions. Dr. A. Rybkin provided some mathematical advice. This study was supported by a grant from the United States National Science Foundation (OPP-9814984) through the Office of Polar Programs, Arctic System Science, and by a fellowship from the Inland Northwest Research Alliance (INRA). The Potsdam Institute for Climate Impact Research graciously provided an office for P. P. Overduin during a portion of writing.

Appendix: List of Symbols

A	constant	--
B	constant	--
C	heat capacity	J kg^{-1} K^{-1}
E_S	effective sensor constant	K s m^{-2}
H	surface thermal conductance	W m^{-2} K^{-1}
J_z	Bessel function of the 1st kind, zth order	--
L_f	latent heat of fusion	J kg^{-1}
P	$= uJ_0(u) + k(hu^2 - \alpha)J_1(u)$	--
Q	heat produced per length of source	W m^{-3}
R	$= uY_0(u) + k(hu^2 - \alpha)Y_1(u)$	--
R_T	thermistor resistance	Ω
S	heat capacity of the heating wire	J m^{-1} K^{-1}
T	temperature of the medium	°C
T_s	heating wire temperature	°C
Y_z	Bessel function of the 2nd kind, zth order	--
b	heat source radius	m
h	Biot number	--
k	thermal conductivity	W m^{-1} K^{-1}
q	heat production per unit length	W m^{-1}
r	radius	m
t	time	s
t_s	time at which heat production ceases	s
u	integration variable	--
z	order, Bessel function	--
ΔT	radial temperature gradient	K m^{-1}
Δ_J	$= J_0(u\eta_1) - J_0(u\eta_2)$	--
Δ_Y	$= Y_0(u\eta_1) - Y_0(u\eta_2)$	--

α	twice the ratio of medium to sensor heat capacities	--
β_i	*i*th parameter in parameter set	i-dependent
χ_i	sensitivity to *i*th parameter	i-dependent
δ_o	resistance offset (thermistors)	Ω
γ	Euler's constant, (0.5772156649)	--
η	ratio of radial position to cylinder radius, *b*	--
κ	medium thermal diffusivity	$m^2\ s^{-1}$
π	pi	--
θ_i	volumetric content of soil component *i*	$m^3\ m^{-3}$
ρ	density	$kg\ m^{-3}$
τ	Fourier number	--
τ_s	dimensionless time at cessation of heat production	--

Subscripts

1, 2	radial positions
app	apparent
i	ice
w	water
s	soil
S	sensor

References

Anisimov, O. A:, Shiklomanov, N. I., Nelson, F. E., 1997. Global warming and active-layer thickness: results from transient general circulation models. Global and Planetary CHange 15: 61-77.

Beck, J. V., Arnold, K.J., 1977. Parameter Estimation. Wiley Sciences.

Beltrami, H., 2001. Surface heat flux histories from inversion of geothermal data: Energy balance at the Earth’s surface. J Geophys Res. 10(B10): 21 979-21 993.

Bittelli, M., Flury, M., Campbell, G. S., 2003. A thermodielectric analyzer to measure the freezing and moisture characteristic of porous media. Water Resour Res. 39(2), doi:10.1029/2001wr000930.

Blackwell, J.H., 1954. A transient flow method for determination of thermal constants of insulating materials in bulk. J Appl Phy. 25: 137-144.

Burt, T. P., Williams, P. J., 1976. Hydraulic Conductivity in Frozen Soils. Earth Surface Processes, 1: 349-360.

Carslaw, H. S., Jaeger, J. C., 1990. Conduction of Heat in Solids, 2nd ed. Clarendon Press, Oxford.

Cull, J. P., 1978. Thermal contact resistance in transient conductivity measurements. J Phys. 11: 323-326.

DeVries, D. A., Peck, A. J., 1958a. On the cylindrical probe method of measuring thermal conductivity with special reference to soils. I Extension of theory and discussion of probe characteristics. Aust J Phys. 11: 255-271.

DeVries, D. A., Peck, A. J., 1958b. On the cylindrical probe method of measuring thermal conductivity with special reference to soils. II Analysis of moisture effects. Aust J Phys. 11: 409-423.

Farouki, O. T., 1981. Thermal properties of soils. Cold Region Research and Engineering Laboratory (CRREL) Monograph 81-1.

Fuchs, M., Campbell, G. S., Papendick, R. I., 1978. An Analysis of Sensible and Latent Heat Flow in a Partially Frozen Unsaturated Soil. Soil Sci Soc Am J. 42(3): 379-385.

Gander, W., Gautschi, W., 1998. Adaptive Quadrature – Revisited. Eidgenössiche Technische Hochschule, Zürich, Report 40: 84-101.

Goodrich, L. E., 1986. Field Measurements of Soil Thermal Conductivity. Can Geotech J. 23: 51-59.

Held, E. F. M. van der, Drunen, F. G. van, 1949. A method of measuring the thermal conductivity of liquids. Physica. 15:865-881.

Hinzman, L. D., Kane, D. L., Gieck, R. E., Everett, K. R., 1991. Hydrologic and thermal properties of the active layer in the Alaskan Arctic. Cold Reg Sci Technol. 19(2): 95-110.

Hinzman, L. D., Goering, D. J., Kane, D. L., 1998. A distributed thermal model for calculating soil temperature profiles and depth of thaw in permafrost regions. J Geophys Res. 103(D22): 28 975-28 991.

Hukseflux Thermal Sensors, 2000. TP01: Thermal Properties Sensor. Delft, Netherlands.

Ippisch, O., 2003. Coupled Transport in Natural Porous Media (2. rev. ed.). Ph. D. Thesis, University of Heidelberg, Germany. http://www.ub.uni-heidelbeg.de/archiv/3320.

Jaeger, J. C., 1956. Conduction of heat in an infinite region bounded internally by a circular cylinder of a perfect conductor. Aust J Phys. 9: 167-169.

Kane, D. L., Hinkel, K. M., Goering, D. J., Hinzman, L. D., Outcalt, S. I., 2001. Non-conductive Heat Transfer Associated With Frozen Soils. Global Planetary Change. 29: 275-292, doi:10.1016/S0921-8181(01)00095-9.

Kane, D. L. and Stein, J., 1983. Water Movement into Seasonally Frozen Soils. Water Resour Res. 19(6): 1547-1557.

Kay, B. D., Fukuda, M., Izuta, H., Sheppard, M. I., 1981. The Importance of Water Migration in the Measurement of the Thermal Conductivity of Unsaturated Frozen Soils. Cold Reg Sci Technol. 5: 95-106.

Kristiansen, J. I., 1982. The transient cylindrical probe method for determination of thermal parameters of earth materials. Geoskrifter 18: 1-154.

Lachenbruch, A., 1957. Measurement of thermal conductivity of frozen soils. T Am Geophys Union. 38(5): 691-697.

Lide, D. R., ed., 2005. CRC Handbook of Chemistry and Physics, CRC Press, Florida.

Loon, W. K. P. van, Perfect, E., Groenevelt, P. H., Kay, B. D., 1991. Application of dispersion theory to time-domain reflectometry. Transport Porous Med. 6: 391-406.

Loon, W. K. P. van, Haneghem, I. A. van, Schenk, J., 1989. A new model for the non-steady-state probe method to measure thermal properties of porous materials. Int J Heat Mass Tran. 32: 1473-1481.

Osterkamp, T. E., 2003. A thermal history of permafrost in Alaska. In: Proceedings of the Eighth International Conference on Permafrost, 21–25 July 2003, Balkema Publishers, Zurich, Switzerland, pp. 863–868.

Overduin, P. P., Ping, C.-L., Kane, D. L., 2003. Frost boils, soil ice content and apparent thermal diffusivity. In: Proceedings of the Eighth International Conference on Permafrost, 21–25 July 2003, Balkema Publishers, Zurich, Switzerland, pp. 863–868.

Ping, C. L., Bockheim, J.G., Kimble, J.M., Michaelson, G.J., Walker, D. A., 1998. Characteristics of cryogenic soils along a latitudinal transect in arctic Alaska. J Geophys Res. 103(D22): 28,917-28,928.

Putkonen, J., 1998. Soil thermal properties and heat transfer processes near Ny Alesund, Northwestern Spitsbergen, Svalbard. Polar Research, 17(2): 165-179.

Putkonen, J., 2003. Determination fo frozen soil thermal properties by heated needle probe. Permafrost and Periglacial Processes 14: 343-347.

Roth, K., Boike, J., 2001. Quantifying the thermal dynamics of a permafrost site near Ny-Ålesund, Svalbard, Water Resour Res. 37(12): doi: 10.1029/ 2000WR000163.

Smith, M. W., Riseborough, D. W., 1985. The sensitivity of thermal predictions to assumptions in soil properties. In: Fourth International Symposium on Ground Freezing, Sapporo, Japan, August 5-7, 1985, pp. 17-23.

Smith, M.W., Tice, A.R., 1988. Measurement of the unfrozen water content of soils-comparison of NMR and TDR methods. CRREL Report, vol. 88-18. US Army Cold Regions Research and Engineering Lab (CRREL).

Soil Survey Staff, 2005. National Soil Survey Characterization Data, Soil Survey Laboratory, National Soil Survey Center, USDA-NRCS - Lincoln, NE.

Topp, G. C., Davis, J. L., Annan, A. P., 1980. Electromagnetic determination of soil water content: Measurement in coaxial transmission lines. Water Resour Res. 16:574-582.

Yershov, E. D., 1990, General Geocryology. Cambridge University Press, 580 pp.

Yoshikawa, K., Bolton, W. R., Romanovsky, V. E., Fukuda, M., Hinzman, L. D., 2003. Impacts of wildfire on the permafrost in the boreal forests of Interior Alaska. J Geophys Res. 108(D1): 8148, doi:10.1029/2001jd000438.

List of Figures

Figure 1. Sensitivities of the radial temperature gradient to the parameters for values b = 8 x 10^{-5} m, S = 131 J m^{-1} K^{-1}, q = 1.5 W m^{-1}, k = 0.3 W m^{-1} K^{-1}, and κ = 2.5 x 10^{-7} m^2 s^{-1}, as a function of time since the beginning of heating. χ_i is defined in the text (equation 20). The left hand axis is for k and κ, the right hand axis for H, b and S. H^{-1} was set to zero for the other five sensitivities, and to 3000 W K^{-1} for χ_H. The units of χ_i depend on i.

Figure 2. Oblique-view schematic diagram of the Hukseflux TP01 thermal properties sensor. The sensor produces a known amount of heat, q, per unit time and length of heating wire along the central heating wire. The temperature difference is measured between radial distances of 1 (r_1) and 5 mm (r_2) from the central heating wire (indicated by q). This temperature difference is averaged over the central 20 mm of the heating wire (longitudinally) and over two angular directions in the plane of the sensor.

Figure 3. The radial temperature difference as a function of time for the first 180 s of heating and then the next 180 s of cooling in four materials is shown. Thermopile and heater voltages are recorded with a datalogger. The former is related to the radial temperature by the thermopile’s Seebeck coefficient. Heat production by the heating wire is related to the resistance of the heating wire, the voltage across it and its length.

Figure 4. The radial temperature difference for times t < 180 s from Figure 3 is plotted here against the inverse of time. Black values are used for the least squares linear fits shown and were selected by calculating the minimum absolute change in correlation coefficient with the addition of each point. The gray points are not used in the linear fit.

Figure 5. Freezing characteristic curve generated using a time domain reflectometry volumetric water content sensor and a temperature sensor proximal to the thermal conductivity sensor discussed here. Data are from a three-year period, 2002-2004, and include three freezing and thawing cycles. Least-square linear fits to the to the data are shown on the graph.

Figure 6. The soil temperature [°C] and fractional volumetric water content [-] are shown in the top graphs, as measured using thermistor and time domain reflectometry sensor. The third graph shows apparent heat capacity, truncated to 6 MJ m^{-3} K^{-1}, calculated using equation 25. The lowest graph shows the apparent thermal conductivity calculated using large times approximations for the line source solution (black), and for the heated cylinder solution (grey).

Figure 7. The apparent thermal conductivities (W m^{-1} K^{-1}) calculated using both the line source approximation (left) and the heated cylinder approximation (right) plotted against soil temperature (°C) from May 18, 2002 until July 21, 2004. Grey circles denote measurements made between February 1 and July 31, while black crosses indicate measurements between August 1 and January 31.

Table 1. Calculated thermal conductivities [W m^{-1} K^{-1}].

Thermal conductivity [W m^{-1} K^{-1}]		Moist Clay (21 °C)	Dry Sand (21 °C)	Ice (-5 °C)	Water and agar gel (21 °C)
Accepted [a]		1.2 – 1.4	0.3 – 0.35	2.38	0.60
Line source approximation		1.36	0.32	1.98	0.59
Line source model [b]		1.31	0.31	1.97	0.53
Heated cylinder approximation	*slope*	1.33 [c]	0.30 [c]	2.08	– [d]
	intercept	1.45	0.34	2.09	– [d]

a – from Yershov (1990) for sand,, clay and water; from Lide (2005) for ice; *b* – the parameter η_1/η_2 is estimated from the manufacturer-provided sensor calibrations; *c* – estimated thermal heat capacities of 1.25 MJ m^{-3} K^{-1} and 2.8 MJ m^{-3} K^{-1} for dry sand and moist clay were taken from Yershov (1990); *d* – used to calculate sensor.

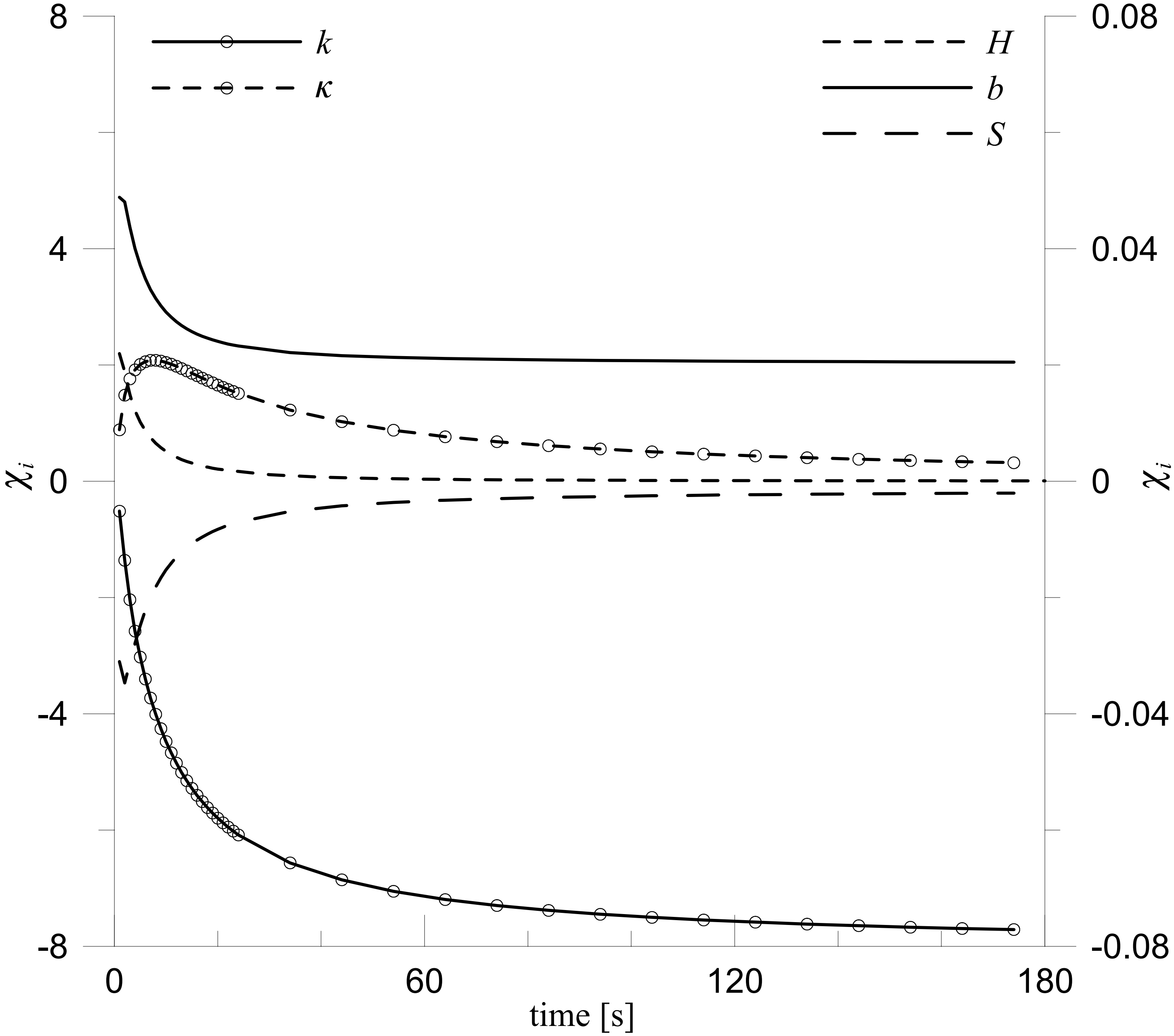

Overduin, Figure 1

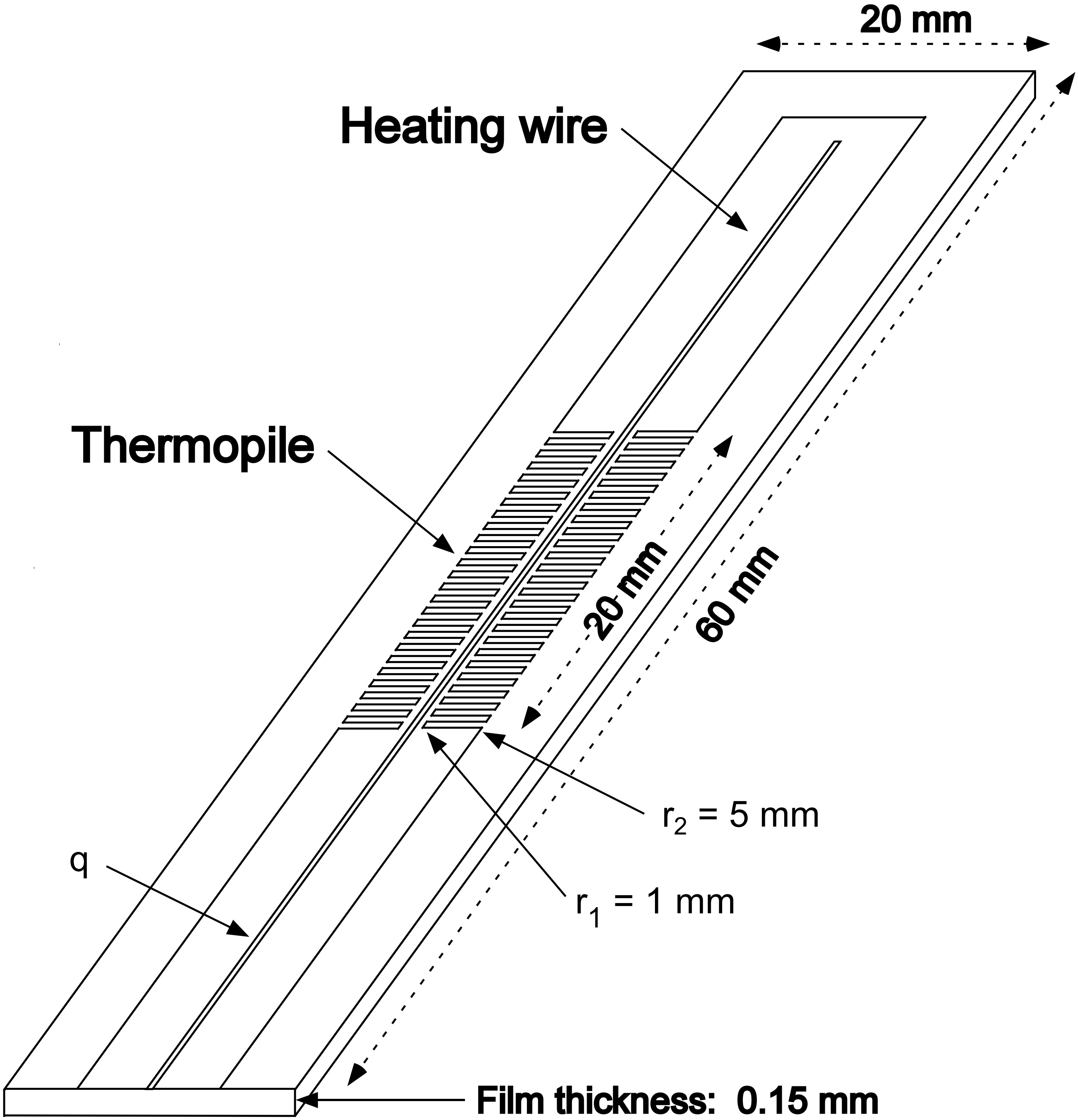

Overduin, Figure 2

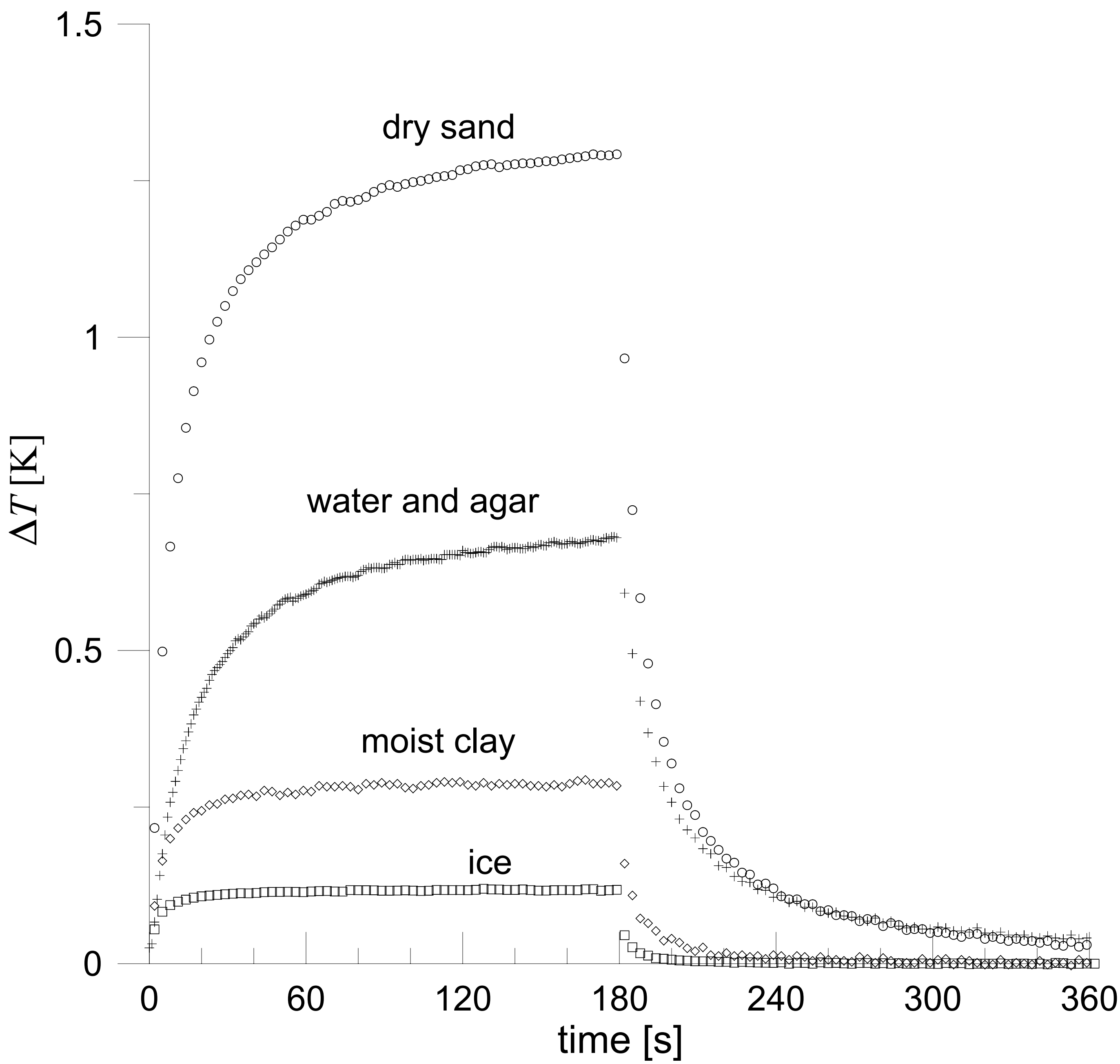

Overduin, Figure 3

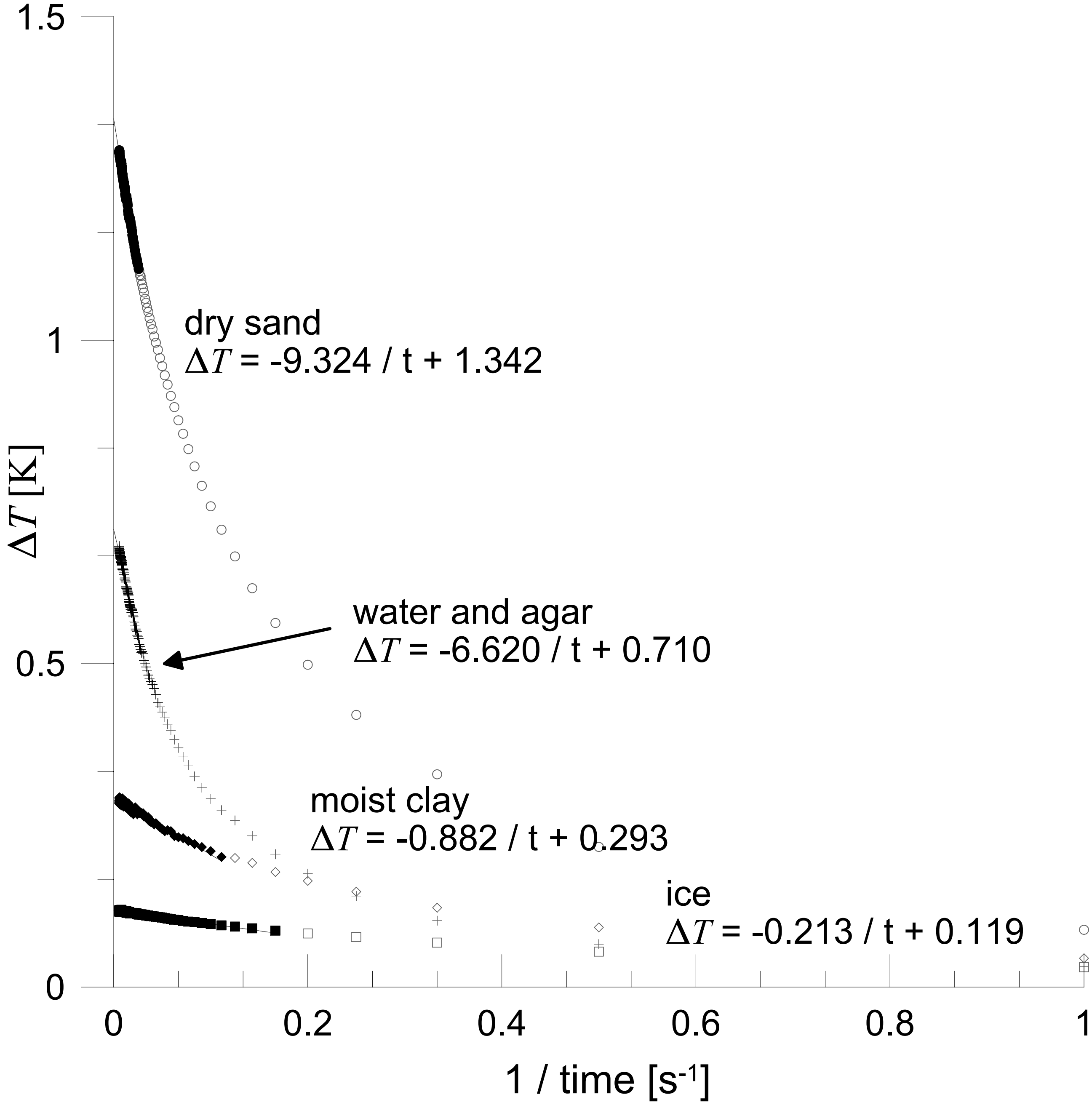

Overduin, Figure 4

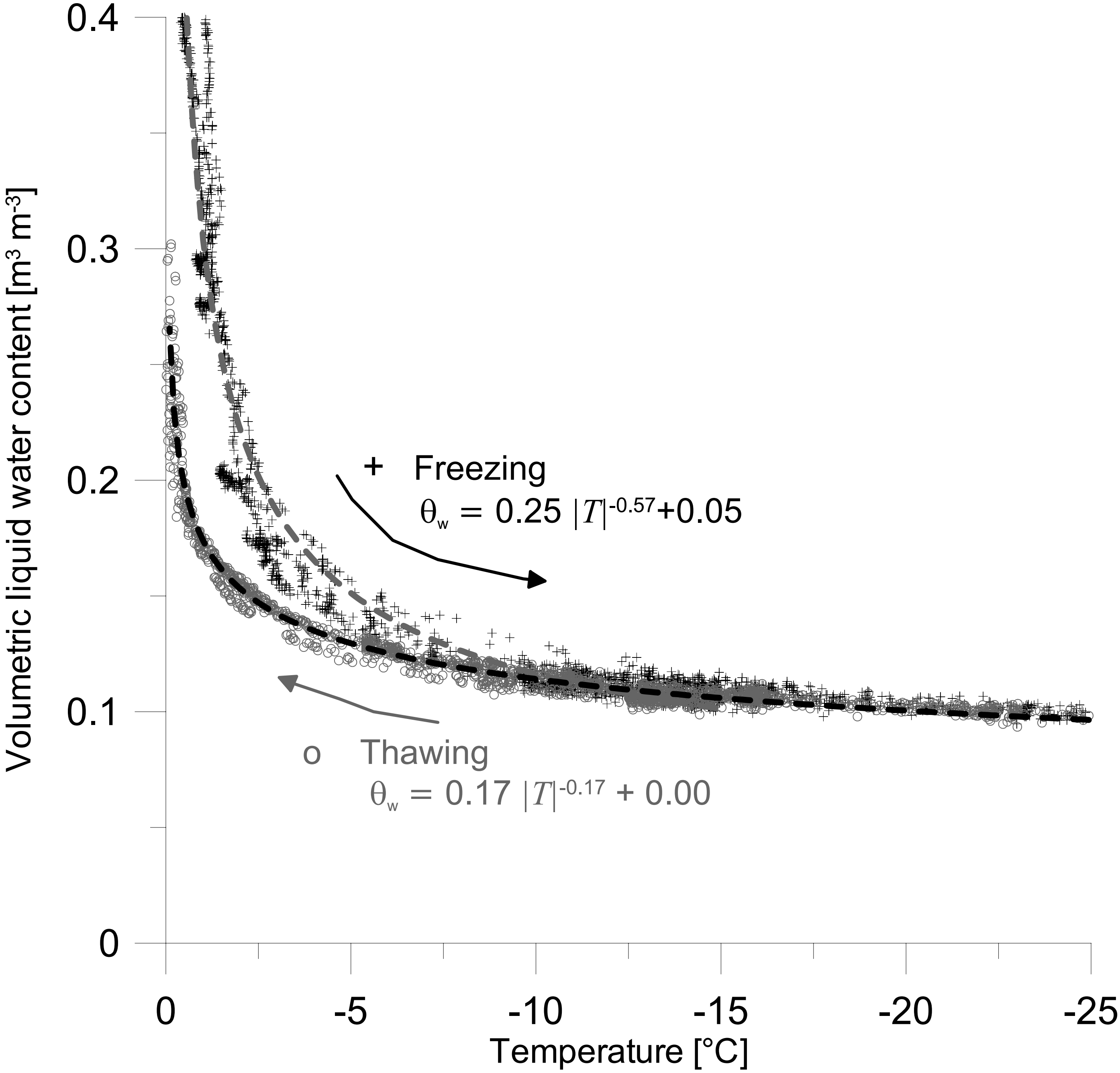

Overduin, Figure 5

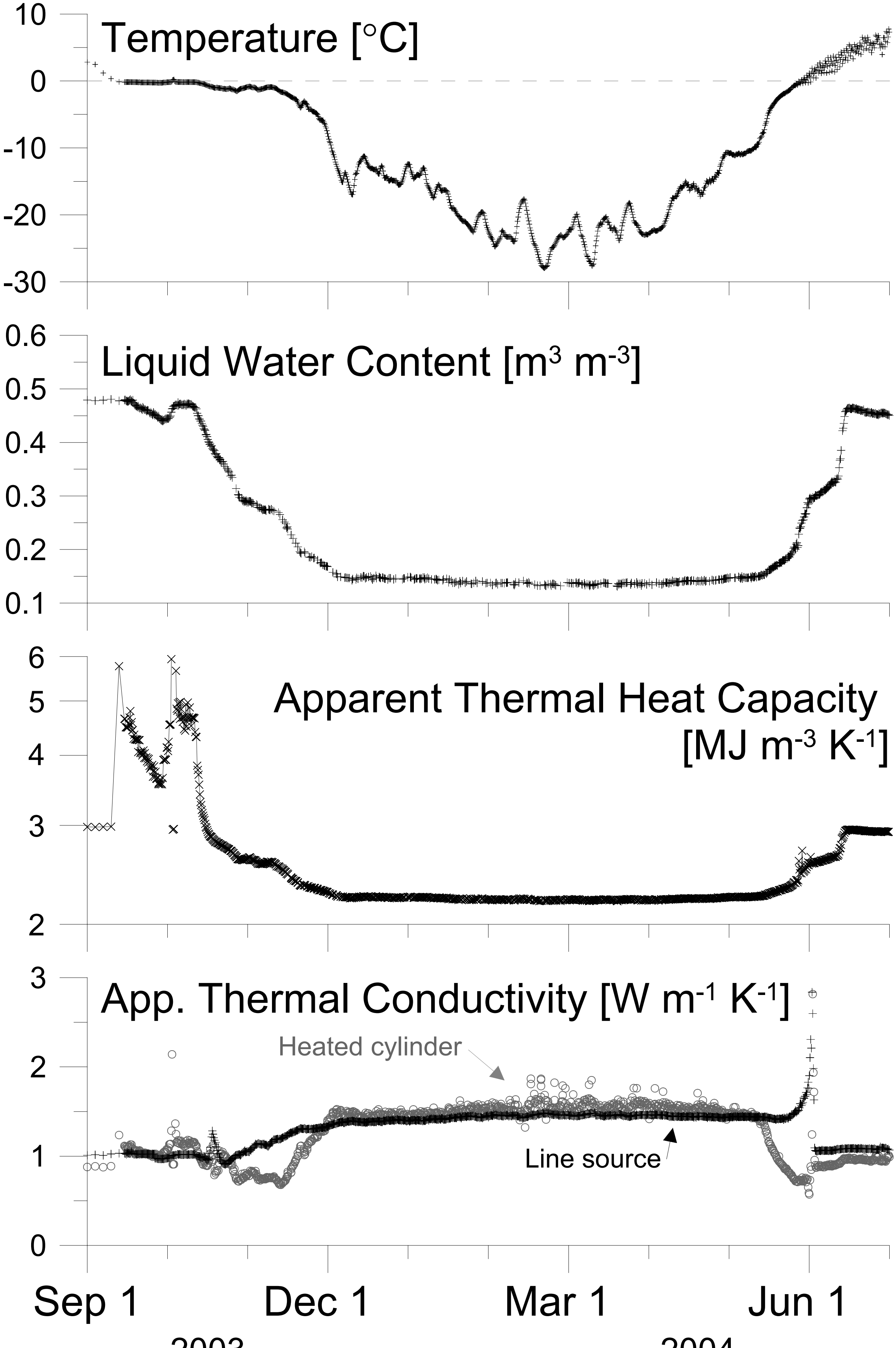

Overduin, Figure 6

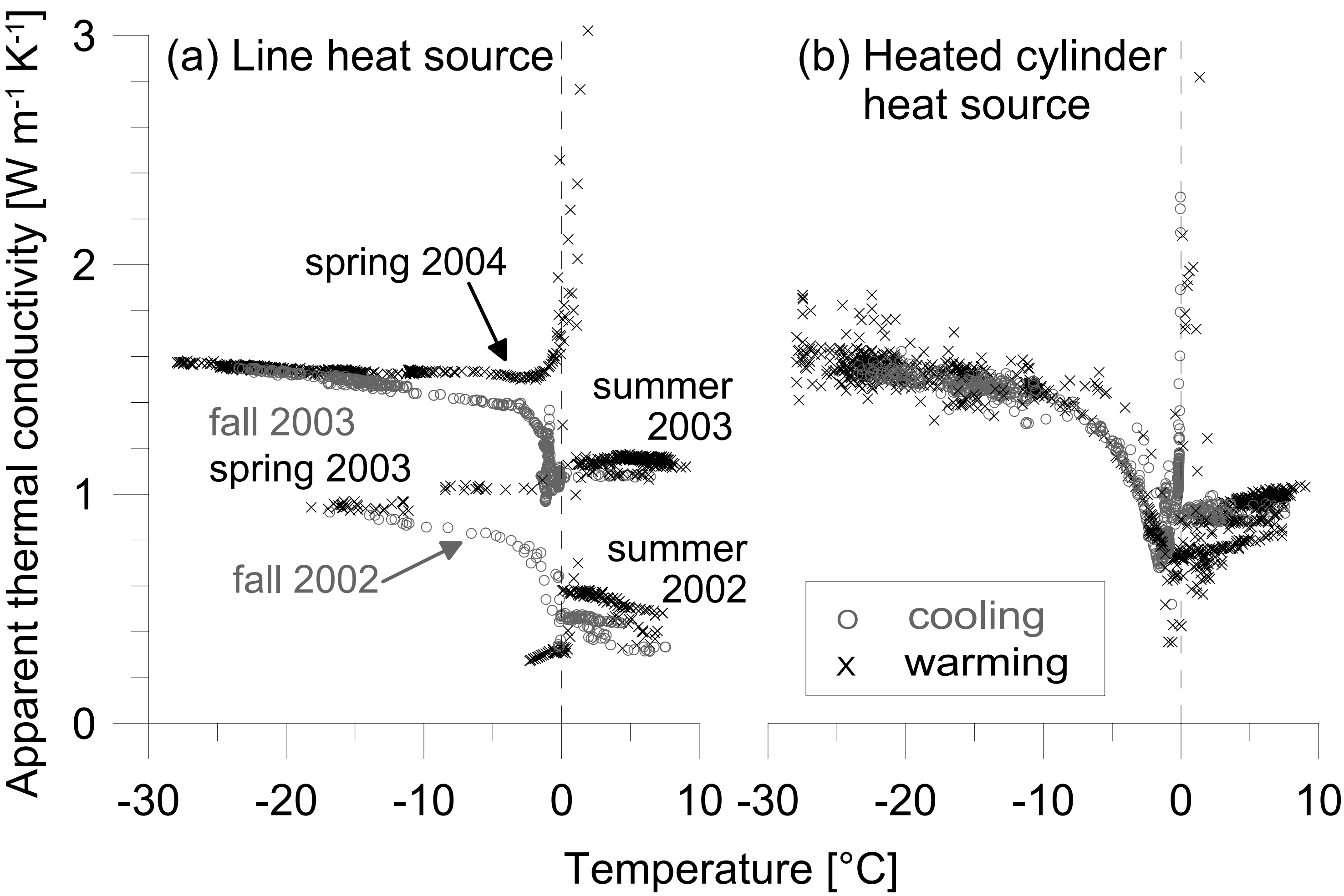

Overduin, Figure 7